Simultaneous Measurement of the Three-Dimensional Orientation of Excitation and Emission Dipoles

ARTICLE *in* PHYSICAL REVIEW LETTERS · OCTOBER 2015

Impact Factor: 7.51 · DOI: 10.1103/PhysRevLett.115.173002

Narain Karedla

Georg-August-Universität Göttingen

Dirk Hähnel

Georg-August-Universität Göttingen

Ingo Gregor

Georg-August-Universität Göttingen

Jörg Enderlein

Georg-August-Universität Göttingen

PRL **115,** 173002 (2015) PHYSICAL REVIEW LETTERS week ending 23 OCTOBER 2015

Simultaneous Measurement of the Three-Dimensional Orientation of Excitation and Emission Dipoles

Narain Karedla, Simon C. Stein, Dirk Hähnel, Ingo Gregor, Anna Chizhik, and Jörg Enderlein[*]
III. Institute of Physics, Georg August University, 37077 Göttingen, Germany

(Received 22 June 2015; published 20 October 2015)

The emission properties of most fluorescent emitters, such as dye molecules or solid-state color centers, can be well described by the model of an oscillating electric dipole. However, the orientations of their excitation and emission dipoles are, in most cases, not parallel. Although single molecule excitation and emission dipole orientation measurements have been performed in the past, no experimental method has so far looked at the *three-dimensional* excitation *and* emission dipole geometry of individual emitters simultaneously. We present the first experimental study, using defocused imaging in conjunction with radially polarized excitation scanning, to measure both the excitation as well as emission dipole orientations of single molecules, which allows us to sample the distribution of their mutual orientation. We find an unexpectedly broad distribution of the angle between both dipoles which we attribute to the interaction between the observed molecules and the substrate they are immobilized on.

DOI: 10.1103/PhysRevLett.115.173002 PACS numbers: 33.70.Ca, 33.80.-b, 42.30.-d, 87.64.-t

Many emission properties of almost all fluorescent organic dyes are well described within the theoretical framework of an ideal electric dipole emitter, which is characterized by an oscillation frequency, dipole strength, and dipole orientation. Even if one takes into account that excitation and emission happens between an ensemble of energy levels in the ground and excited states, resulting in broad excitation and emission spectra, a molecule's excitation and emission properties are still excellently modeled by a superposition of dipole transitions having different oscillation frequencies but the same orientation. This orientation plays a crucial role in defining the photophysical properties of a molecule in an anisotropic environment such as close to a surface or in a nanocavity [1,2], or in Förster resonance energy transfer [3,4]. For most fluorescent molecules, the excitation and emission dipole orientations are not collinear but are inclined to each other. This is well known from fluorescence anisotropy measurements where the angle between the excitation and emission dipole enters the expression for the fundamental anisotropy of a fluorescing molecule [5]. While it is rather straightforward to determine the projection of an excitation or emission dipole into a plane perpendicular to the excitation or detection axis, by using polarized excitation and detection [6,7], the determination of the full three-dimensional orientation is more difficult. Several methods have been developed for measuring the three-dimensional orientation of the emission dipole of single molecules. Among them are aberrated imaging [8], polarized evanescent field excitation and imaging [9,10], defocused imaging [11,12], or Bertrand lens imaging [13]. Other methods are based on redistributing the collected emission in a way that allows the separate detection of emission into different solid angles [14–16]. More recently, methods based on wave-front engineering of emitted light by phase plates, quadrated pupils, or spatial light modulators have been used for determining the emission dipole orientation [17–19].

Most techniques for measuring the three-dimensional orientation of the excitation dipole of a single emitter are based on scanning a molecule with a focused laser beam with temporally or spatially varying electric field polarization [20–25]. The simplest of these methods is to scan a molecule with a radially polarized doughnut excitation focus [26,27]. Because of the inhomogeneous longitudinal and transversal polarization components across such a focus, each single-molecule scan shows a characteristic intensity pattern which depends on the three-dimensional orientation of its excitation dipole.

Many of the above mentioned techniques have also been used to successfully determine the dimensionality and geometry of the excitation and emission transitions in fluorescent nanocrystals (quantum dots), and to characterize their behavior in complex electromagnetic environments [28–34]. However, until now, there exists no study which determines both the three-dimensional excitation and emission dipole orientations of single emitters simultaneously, which would allow for obtaining distribution functions of the relative angle between both dipoles.

In this Letter, we present the first experimental study which looks at the three-dimensional orientations of both the excitation as well as emission dipoles of single immobilized dye molecules. Figure 1 shows a schematic representation of the optical setup. A white-light laser (SC400-4-80, Fianium) together with an acousto-optic tunable filter (AOTFnC-400.650-TN, AA Opto-Electronic) was used for excitation. The linearly polarized TEM_{00} beam was then passed through a liquid-crystal mode converter (ARCoptix) which rotates the light polarization in a position-dependent manner to generate a radially polarized TEM_{01} beam. A 25 μm pinhole was used for mode cleaning and to block unwanted higher orders of vortex modes that are also generated by the mode converter. This beam was then reflected with a nonpolarizing beam splitter (BS019, ThorLabs) into an objective lens with high numerical aperture (APON60XOTIRF, 1.49 N.A., oil immersion, Olympus) which focused the beam onto the surface. A nonpolarizing beam splitter, instead of a more conventional dichroic mirror, was used to exclude all potential polarization effects upon reflection or transmission which are typically observed with dichroic mirrors.

As a first sample, we studied individual molecules of the dye Atto 655 (Atto-Tec) spin coated from a 1 nM aqueous dye solution on top of a cleaned glass (refractive index 1.52) coverslip. Scanning was done by moving the sample with a piezoelectric stage with scan steps of 50 nm. Collected fluorescence photons were focused onto the active area of a single-photon avalanche photodiode (PicoQuant τ-SPAD) and counted with a multichannel picosecond event timer (HydraHarp 400, PicoQuant). The backscattered excitation light was blocked using a long pass filter (BLP01-635R, Semrock) and an additional band pass filter (FF01-692/40, Semrock). Excitation laser power, ~4 kW/cm^2, and sample scan rate, 3 ms per scan step, were chosen in such a way as to minimize photobleaching and to achieve a reasonable signal-to-noise ratio in the excitation images. After recording a scan image of a large area with many single molecules, the excitation focus was sequentially parked on each molecule's position, identified from the scan image, and the collected fluorescence was guided, with a replaceable mirror, onto an electron-multiplying CCD camera (EMCCD) (iXon DU860-D, Andor Technology). For the chosen magnification, the pixel size of the camera corresponds to a 60×60 nm area in sample space. The camera was shifted along the optical axis away from the sample to achieve defocused imaging with a defocusing value of about 0.9 μm in object space (camera displacement divided by the square of lateral magnification). Each image was acquired with an exposure time of 9 s, an EM gain of 100, and an excitation power of ~10 kW/cm^2. All data collection and hardware synchronization were performed using LabVIEW.

The excitation-focus polarization contains a strong longitudinal field component together with a radial transverse field as shown in Fig. 1. The fluorescence intensity distribution across the scan image of a single emitter can be

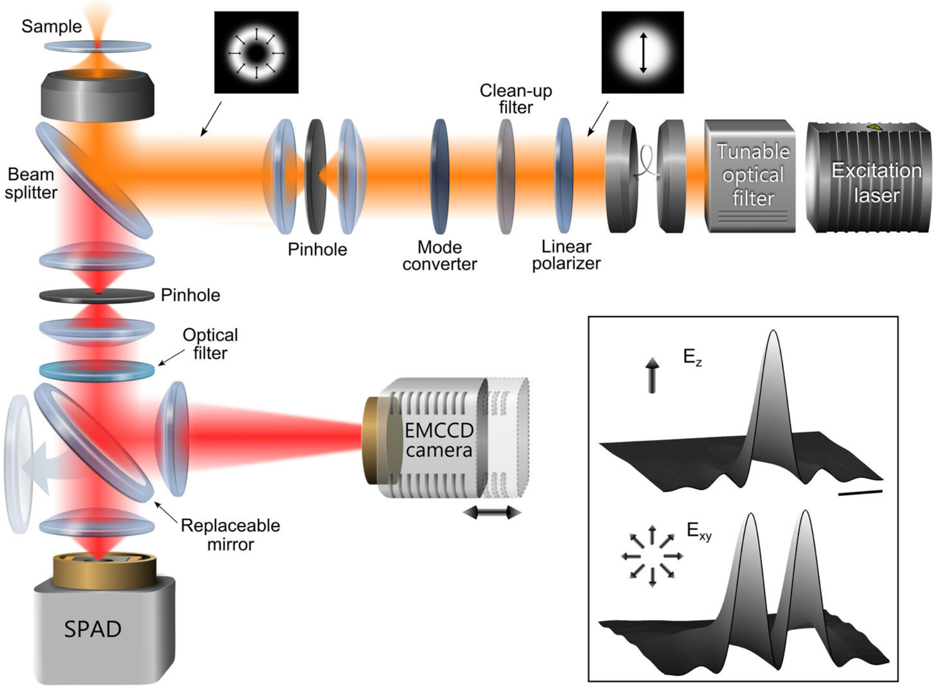

FIG. 1 (color online). Experimental setup showing the path of the excitation beam and the fluorescence emission pathways. The collimated pulsed laser TEM_{00} is passed through a linear polarizer. Any unwanted wavelengths were blocked using a clean-up filter before the beam was passed through the mode converter. Next, the beam was mode cleaned by focusing it through a 25 μm pinhole, resulting in a doughnut profile of radially polarized light. The beam splitter reflected this light beam into an objective which focused the light onto the sample. The inset shows the calculated longitudinal and transverse electric field components on the surface of the substrate 0.5 μm around the optical axis (scalebar = 200 nm). The sample is first scanned with a single-photon avalanche photodetector (SPAD) as detector, to obtain excitation dipole images of the emitters. Subsequently, a replaceable mirror is switched into the detection pathway to reflect the emission onto an EMCCD camera which is displaced away from the imaging plane, to obtain defocused images of the emission dipoles.

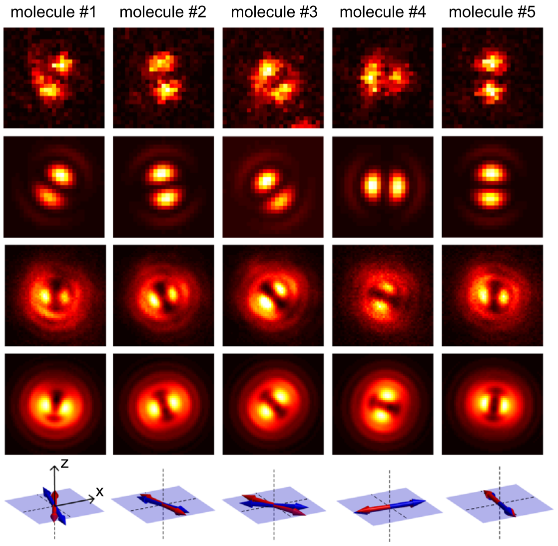

FIG. 2 (color online). Emission and excitation patterns of five Atto 655 molecules. The top row shows the excitation images, the second row the corresponding fitted patterns, the third row shows the defocused images, and the fourth row the fitted emission patterns. The scan pixel size is 50 nm and each excitation image is 25 × 25 pixels, whereas the camera pixel size is ~60 nm, with each defocused image having 40 × 40 pixels. The last row is a depiction of both the excitation (light) and emission (dark) dipole orientations, as fitted from the measurements. The θ and the ϕ values indicate the orientation with respect to the z and x axes, shown for the first molecule. The fitted orientation angles for both dipoles are shown in Table I.

written as $I_f \propto |\mathbf{E}(\mathbf{r}) \cdot \boldsymbol{\mu}_{\text{exc}}|^2$, where $\mathbf{E}(\mathbf{r})$ is the position-dependent electric field in the focus and $\boldsymbol{\mu}_{\text{exc}}$ is the excitation dipole vector. Because of the peculiar polarization structure of the focused field of a radially polarized laser beam, each scan image shows a unique spatial distribution pattern based on its excitation dipole orientation [22]. The top row in Fig. 2 shows five such excitation patterns obtained from the scans. With the chosen laser power and scanning rate, the total number of photons collected from each molecule ranged from 1×10^3 to 4.5×10^3.

Close to an interface dividing two media with different refractive index values, the angular distribution of radiation of an emitter deviates considerably from the $\sin^2 \Theta$ distribution (where Θ is the angle between emission dipole axis and direction of observation) that is observed in a homogeneous environment [35]. Nonpropagating near-field components of the dipole's emission field can tunnel into the optically denser medium and become propagating, leading to radiation above the critical angle of total internal reflection (supercritical angle fluorescence) [36]. When imaging this emission with a high-N.A. objective onto a defocused camera, one observes a characteristic defocused single-molecule image with an intensity distribution which depends on the three-dimensional orientation of the molecule's emission dipole [11]. Defocused images of single Atto 655 molecules are shown in the third row in Fig. 2. We estimated the number of photons in each pixel by converting the EMCCD counts into photon numbers, taking into account the used electron-multiplying gain and the sensitivity of the camera. It was done by first subtracting from the recorded camera counts the camera bias, multiplying the result with the sensitivity (average number of photons required to produce one count, which depends on the preamp setting and the read-out rate), and then dividing it by the electron gain used. The total number of photons detected per molecule ranged from 1.6×10^5 to 1.2×10^6, which spread over an area of $\sim 40 \times 40$ pixels.

TABLE I. Orientation angles of excitation and emission dipoles for the five molecules shown in Fig. 2.

Molecule No.	ϕ_{exc}	θ_{exc}	ϕ_{em}	θ_{em}
1	61°	83°	86.6°	76.4°
2	102°	89°	288.8°	87.9°
3	125°	83°	315.9°	87.0°
4	357°	89°	162.7°	83.8°
5	87°	88°	82.2°	88.1°

For data evaluation, wave-optical calculations were performed to compute a discrete set of theoretical excitation scan images [26,37,38] and defocused wide field images [11,39] for azimuthal, ϕ, and polar angles, θ, in 5° steps. These master patterns were used to find and fit the single-molecule intensity images using a least-squares minimizing pattern matching algorithm [39] by shifting the patterns in steps of one pixel over the recorded image. The obtained fit parameters served as the initial guess values for the optimization of a Poissonian-noise based log-likelihood function [40]

$$L = -\sum_{\mathbf{r}} \{ I(\mathbf{r}) \cdot \log\,[A\,P(\mathbf{r}|\mathbf{r}_P, \phi, \theta) + B]) - [A\,P(\mathbf{r}|\mathbf{r}_P, \phi, \theta) + B] \}, \tag{1}$$

which yields refined parameters beyond the discrete set of values recovered by the pattern matching. Here, $I(\mathbf{r})$ denotes the measured image and $P(\mathbf{r}|\mathbf{r}_P, \phi, \theta)$ is the pattern calculated using the same wave-optical model as before. The optimization was done for the parameters $\mathbf{r}_P, \phi, \theta, A, B$, where $\mathbf{r}_P$ is the pattern's central position, A the integrated intensity, and B the background intensity. The optimization algorithm was based on the a conjugate gradient method. Refinement of the fit using the log-likelihood function increases the fit accuracy by five to tenfold. Theoretically, one could use, for the pattern matching, a set of patterns with a tenfold finer angular spacing of θ and ϕ values, which would make the log-likelihood-based refinement obsolete. However, such an approach would be computationally prohibitive.

The second and fourth rows of Fig. 2 show the fitted excitation and emission patterns for five molecules. To estimate the fitting errors, we applied a bootstrap algorithm where new noisy samples were generated based on the estimated parameters, and then fitted again. In this way, a distribution for each parameter was obtained by fitting one thousand resampled images using the above maximum likelihood estimator. The θ values for almost all molecules were close to 90°, which indicates that the spin-coated molecules were lying mostly flat on the substrate [41].

The mean errors of θ and ϕ for the orientation of $\boldsymbol{\mu}_{\mathrm{exc}}$ are both better than $\pm 2°$, whereas for the orientation of $\boldsymbol{\mu}_{\mathrm{em}}$, they are both better than $\pm 0.4°$. These small values of the standard deviations for the obtained angles are due to the high total number of detected photons per molecule. After obtaining the orientations of both $\boldsymbol{\mu}_{\mathrm{exc}}$ and $\boldsymbol{\mu}_{\mathrm{em}}$, the inclination angle β between excitation and emission dipoles was calculated for each molecule. Figure 3 shows the distribution of β for 25 measured Atto 655 molecules. The β values vary between 7° and 33° with a mean of ~15° which shows that there is a significant variation of the relative orientations of $\boldsymbol{\mu}_{\mathrm{exc}}$ and $\boldsymbol{\mu}_{\mathrm{em}}$. We attribute this wide variation of the β values to a bending of the molecule's backbone structure due to its interaction with the surface (electrostatic and van der Waals interactions). For comparison, we performed conventional time-resolved anisotropy measurements [5] on a bulk solution (1 μM) of the dye in glycerol (to slow down rotational diffusion) using a commercial time-resolved fluorescence spectrometer (MicroTime 200, PicoQuant) with a low-aperture air objective (0.75 N.A., 20×, Olympus) for minimizing any objective-related depolarization effects. We determined a fundamental anisotropy value r_0 of 0.361 which translates into an angle β [see Eq. (10.22) in Ref. [5]] between excitation and emission dipole of 14.9°, in excellent agreement with the mean value seen in the distribution of Fig. 3.

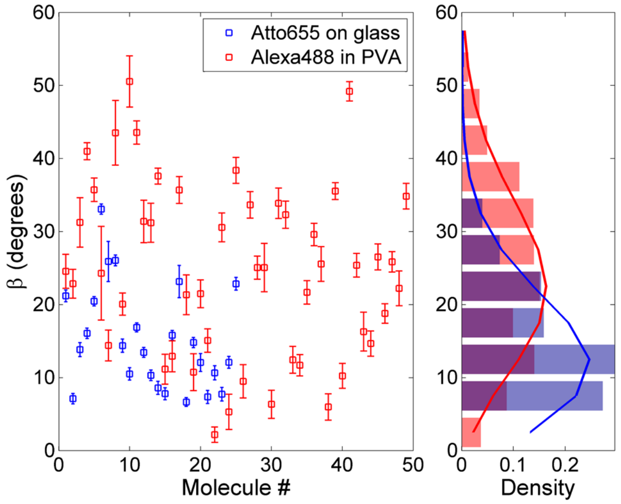

FIG. 3 (color online). Determined β values (left) and their corresponding distribution (right) for 25 measured Atto 655 molecules on a glass surface (blue), and for 49 Alexa 488 molecules embedded into a polymer film (red). The error bars shown in the left figure were estimating using a bootstrapping algorithm. The right side shows the probability distributions with a bin width of 5°. The distributions were fitted with a Poisson distribution (solid lines) yielding a mean value of β equal to 14.6° for Atto 655 and equal to 22.5° for Alexa 488. The results for the first five molecules of Atto 655 correspond to the five measurements shown in Fig. 2 and listed in Table I.

As a second system, we investigated molecules of the dye Alexa 488 (Invitrogen) embedded into a thin layer of polymer by spin coating a 0.1% w/v polyvinyl alcohol (PVA/water, refractive index 1.55) solution containing 1 nM of the dye on top of a cleaned coverslip at 6000 rpm for 60 s, yielding a distribution of immobilized single molecules within a polymer film of less than 100 nm thickness. The sample was excited with an excitation power of 1.6 kW/cm^2 at 485 nm and a scan rate similar to the previous measurements. As before, backscattered excitation light was blocked using suitable long (BLP01-488R, Semrock) and band pass (FF02-525/40, Semrock) filters. The defocused images were obtained at the same excitation power but with the camera set to a position such that the effective defocusing at the object space was around 0.6 μm, and the acquisition time was now 15 s. The total number of photons collected from the Alexa 488 molecules ranged between 2×10^4 and 1.5×10^5 on the defocused camera, while between 0.7×10^3 and 3.4×10^3 in the excitation scan images. Now, the determined θ values showed a broad distribution between 0° and 90° indicating that the molecules immobilized within the polymer layer did not have any longer a preferred orientation parallel to the surface, as was seen for the Atto 655 sample which had been spin coated from an aqueous solution onto the glass surface. The mean errors of θ and ϕ for $\boldsymbol{\mu}_{\mathrm{exc}}$ are around $\pm 5°$, whereas for $\boldsymbol{\mu}_{\mathrm{em}}$ they are around $\pm 1°$. The difference in accuracy between the Atto 655 and the Alexa 488 measurements can be explained by (i) the low number of total photons that were collected from the Alexa 488 dye molecules, and (ii) the smaller defocusing value chosen in order to achieve a better signal-to-noise ratio, which effects the accuracy of estimating the θ and ϕ values, in particular, for dipoles oriented almost vertically to the plane of the substrate. The distribution of the β values for the Alexa 488 sample varies between 2° and 51° and is also shown in Fig. 3. We used the same bootstrapping method as before for estimating the errors of the β values. The Alexa 488 sample shows a larger mean value and broader distribution for β angles as compared to the Atto 655 sample. Again, we used time-resolved anisotropy measurements on a dye solution in glycerol to determine a value of β of 19.9°, close to the mean value found for distribution in Fig. 3.

In conclusion, we have presented a method which measures the three-dimensional orientation of both the excitation as well as emission dipoles of single dipolar emitters. It should be noted that the method gives absolute values with no degeneracy, except for the physical ambiguity of the dipole orientation—a dipole does not have a directed orientation like a vector, but only singles out a line in three-dimensional space. Finally, the presented method of simultaneously taking scan images with radially polarized laser focus and recording defocused wide field images can be extended to study more exotic emitters such as magnetic dipoles, electric multipoles, or quantum dots with complex multidimensional dipole structure.

Financial support by the Deutsche Forschungsgemeinschaft is gratefully acknowledged (SFB 860, project A6, and SFB 937, projects A7 and A11). A. M. C. thanks the Dorothea Schlözer Fellowship Programme for financial support.

---

[*] jenderl@gwdg.de

[1] A. I. Chizhik, I. Gregor, F. Schleifenbaum, C. B. Müller, C. Röling, A. J. Meixner, and J. Enderlein, Phys. Rev. Lett. **108**, 163002 (2012).
[2] A. I. Chizhik, I. Gregor, B. Ernst, and J. Enderlein, ChemPhysChem **14**, 505 (2013).
[3] S. Weiss, Science **283**, 1676 (1999).
[4] T. Ha, A. Y. Ting, J. Liang, W. B. Caldwell, A. A. Deniz, D. S. Chemla, P. G. Schultz, and S. Weiss, Proc. Natl. Acad. Sci. U.S.A. **96**, 893 (1999).
[5] J. R. Lakowicz, *Principles of Fluorescence Spectroscopy* (Springer Science & Business Media, New York, 2007).
[6] T. Ha, T. Enderle, D. S. Chemla, P. R. Selvin, and S. Weiss, Phys. Rev. Lett. **77**, 3979 (1996).
[7] T. Ha, T. A. Laurence, D. S. Chemla, and S. Weiss, J. Phys. Chem. B **103**, 6839 (1999).
[8] A. P. Bartko and R. M. Dickson, J. Phys. Chem. B **103**, 11237 (1999).
[9] R. M. Dickson, D. J. Norris, and W. E. Moerner, Phys. Rev. Lett. **81**, 5322 (1998).
[10] J. N. Forkey, M. E. Quinlan, and Y. E. Goldman, Biophys. J. **89**, 1261 (2005).
[11] M. Böhmer and J. Enderlein, J. Opt. Soc. Am. B **20**, 554 (2003).
[12] J. Jasny and J. Sepioł, Chem. Phys. Lett. **273**, 439 (1997).
[13] M. A. Lieb, J. M. Zavislan, and L. Novotny, J. Opt. Soc. Am. B **21**, 1210 (2004).
[14] J. Hohlbein and C. G. Hübner, Appl. Phys. Lett. **86**, 121104 (2005).
[15] C.-Y. Lu and B. D. Vanden, J. Chem. Phys. **128**, 244501 (2008).
[16] S. Stallinga and B. Rieger, Opt. Express **20**, 5896 (2012).
[17] Z. Sikorski and L. M. Davis, Opt. Express **16**, 3660 (2008).
[18] A. S. Backer, M. P. Backlund, A. R. von Diezmann, S. J. Sahl, and W. Moerner, Appl. Phys. Lett. **104**, 193701 (2014).
[19] M. R. Foreman, C. M. Romero, and P. Török, Opt. Lett. **33**, 1020 (2008).
[20] M. Prummer, B. Sick, B. Hecht, and U. P. Wild, J. Chem. Phys. **118**, 9824 (2003).
[21] E. Betzig and R. J. Chichester, Science **262**, 1422 (1993).
[22] L. Novotny, M. R. Beversluis, K. S. Youngworth, and T. G. Brown, Phys. Rev. Lett. **86**, 5251 (2001).
[23] B. Sick, B. Hecht, U. Wild, and L. Novotny, J. Microsc. **202**, 365 (2001).
[24] A. Débarre, R. Jaffiol, C. Julien, D. Nutarelli, A. Richard, P. Tchénio, F. Chaput, and J.-P. Boilot, Eur. Phys. J. D **28**, 67 (2004).
[25] M. P. Backlund, M. D. Lew, A. S. Backer, S. J. Sahl, G. Grover, A. Agrawal, R. Piestun, and W. Moerner, Proc. Natl. Acad. Sci. U.S.A. **109**, 19087 (2012).
[26] A. I. Chizhik, A. M. Chizhik, A. Huss, R. Jäger, and A. J. Meixner, J. Phys. Chem. Lett. **2**, 2152 (2011).
[27] A. M. Chizhik, R. Jäger, A. I. Chizhik, S. Bär, H.-G. Mack, M. Sackrow, C. Stanciu, A. Lyubimtsev, M. Hanack, and A. J. Meixner, Phys. Chem. Chem. Phys. **13**, 1722 (2011).
[28] A. I. Chizhik, A. M. Chizhik, D. Khoptyar, S. Bär, and A. J. Meixner, Nano Lett. **11**, 1131 (2011).
[29] T. H. Taminiau, F. D. Stefani, and N. F. van Hulst, Opt. Express **16**, 10858 (2008).
[30] S. A. Empedocles, R. Neuhauser, K. Shimizu, and M. G. Bawendi, Adv. Mater. **11**, 1243 (1999).
[31] X. Brokmann, L. Coolen, J.-P. Hermier, and M. Dahan, Chem. Phys. **318**, 91 (2005).
[32] K. Early, K. McCarthy, M. Odoi, P. Sudeep, T. Emrick, and M. Barnes, ACS Nano **3**, 453 (2009).
[33] A. G. Curto, G. Volpe, T. H. Taminiau, M. P. Kreuzer, R. Quidant, and N. F. van Hulst, Science **329**, 930 (2010).
[34] D. Patra, I. Gregor, J. Enderlein, and M. Sauer, Appl. Phys. Lett. **87**, 101103 (2005).
[35] E. H. Hellen and D. Axelrod, J. Opt. Soc. Am. B **4**, 337 (1987).
[36] T. Ruckstuhl and D. Verdes, Opt. Express **12**, 4246 (2004).
[37] D. Khoptyar, R. Gutbrod, A. Chizhik, J. Enderlein, F. Schleifenbaum, M. Steiner, and A. J. Meixner, Opt. Express **16**, 9907 (2008).
[38] R. Gutbrod, D. Khoptyar, M. Steiner, A. M. Chizhik, A. I. Chizhik, S. Bär, and A. J. Meixner, Nano Lett. **10**, 504 (2010).
[39] D. Patra, I. Gregor, and J. Enderlein, J. Phys. Chem. A **108**, 6836 (2004).
[40] K. I. Mortensen, L. S. Churchman, J. A. Spudich, and H. Flyvbjerg, Nat. Methods **7**, 377 (2010).
[41] N. Karedla, A. I. Chizhik, I. Gregor, A. M. Chizhik, O. Schulz, and J. Enderlein, ChemPhysChem **15**, 705 (2014).